

Multi-Scale Representation Learning for Image Restoration with State-Space Model

Yuhong He^{*1}, Long Peng^{*}, Qiaosi Yi^{3†}, Chen Wu², Lu Wang^{1†}

¹Northeastern University, China

²University of Science and Technology of China

³The Hong Kong Polytechnic University

Abstract

Image restoration endeavors to reconstruct a high-quality, detail-rich image from a degraded counterpart, which is a pivotal process in photography and various computer vision systems. In real-world scenarios, different types of degradation can cause the loss of image details at various scales and degrade image contrast. Existing methods predominantly rely on CNN and Transformer to capture multi-scale representations. However, these methods are often limited by the high computational complexity of Transformers and the constrained receptive field of CNN, which hinder them from achieving superior performance and efficiency in image restoration. To address these challenges, we propose a novel Multi-Scale State-Space Model-based (MS-Mamba) for efficient image restoration that enhances the capacity for multi-scale representation learning through our proposed global and regional SSM modules. Additionally, an Adaptive Gradient Block (AGB) and a Residual Fourier Block (RFB) are proposed to improve the network’s detail extraction capabilities by capturing gradients in various directions and facilitating learning details in the frequency domain. Extensive experiments on nine public benchmarks across four classic image restoration tasks, image deraining, dehazing, denoising, and low-light enhancement, demonstrate that our proposed method achieves new state-of-the-art performance while maintaining low computational complexity. The source code will be publicly available.

Introduction

In the process of real-world image transmission, images are inevitably degraded by various factors such as noise, low-light, and adverse weather conditions (Yu et al. 2022; Mao et al. 2021). These types of degradation significantly impair image visibility (Khudjaev et al. 2024) and negatively impact downstream vision tasks like autonomous driving (Zhang et al. 2023) and surveillance (Qu et al. 2024). Image restoration, a fundamental task in image processing, aims to reconstruct high-quality and detail-rich images from degraded inputs (Shen et al. 2023; Chen et al. 2018; Zamir et al. 2020a). In real-world scenarios, different degradation patterns lead to detail and contrast loss at various scales.

^{*}These authors contributed equally.

[†]Lu Wang and Qiaosi Yi are the corresponding authors.

Copyright © 2025, Association for the Advancement of Artificial Intelligence (www.aaai.org). All rights reserved.

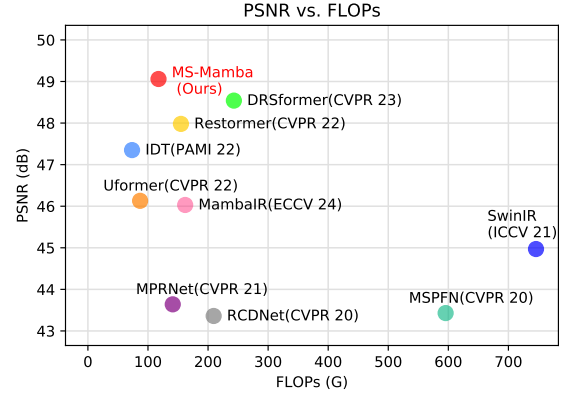


Figure 1: Model complexity and performance comparison between our MS-Mamba and existing state-of-the-art and classic image restoration methods on the SPA-Data dataset. Our method achieves superior performance while maintaining lower computational costs.

For instance, noise disrupts the fine textures of images (Ren et al. 2021; Mou, Zhang, and Wu 2021), whereas the different scales of raindrops and rain streaks degrade multi-scale details of images (Fu et al. 2021; Wang et al. 2020). Additionally, adverse conditions such as hazy weather and low-light conditions further complicate the extraction of details and contrast (Ye et al. 2022; Yang et al. 2021a). Therefore, numerous methods have been proposed to capture contextual information across different scales and model the relationships between them to enhance the details and contrast of the restored images (Yin, Tu, and Chen 2023; Tu et al. 2022; Li, Chen, and Chang 2023).

Specifically, previous methods introduce multi-scale convolutional neural network (CNN) modules to enhance the perception of multi-scale information (Jiang et al. 2020; Mehri, Ardakani, and Sappa 2021). However, these modules primarily focus on local feature extraction and struggle to capture global information. To overcome these limitations, researchers propose employing the self-attention mechanism through Transformers to effectively model long-range global features. (Song et al. 2023; Xiao et al. 2022; Cai et al. 2023). These approaches enable networks to capture global contextual information, providing new perspectives and possibilities for multi-scale representation learning. Recognizing the distinct advantages of Transformers and CNN in

modeling long-range dependencies and local features, researchers propose hybrid CNN-Transformer modules to develop multi-scale architecture (Chen et al. 2023; Brateanu et al. 2024). Although hybrid CNN-Transformer methods facilitate networks in handling degradation patterns in complex real-world scenes, they still face the following challenges: a) Transformers have high computational costs and complexity, particularly when processing high-resolution images (Liang et al. 2021; Guo et al. 2022). b) CNN struggles to provide rich local features, which limits its ability to model middle-scale (i.e., regional-level) features (Liu et al. 2021; Zamir et al. 2020b; Soh and Cho 2022).

To address these challenges, we revisit multi-scale representation learning in image restoration and propose a novel Multi-Scale SSM-based (MS-Mamba) representation learning network. It can achieve the best image restoration performance while maintaining low computational cost and high efficiency, as shown in Fig. 1. Specifically, we propose a novel Hierarchical Mamba Block (HMB), which can enhance the network’s capacity for multi-scale representation through the integration of global and regional State-Space Model (SSM) modules and efficient local CNN. In HMB, to efficiently learn global features, we design a global SSM module. This module leverages efficient state-space functions to enhance the network’s ability to capture global contextual information. To effectively learn regional-level features, we innovatively propose a regional SSM module in HMB, which integrates multi-scale attention mechanisms within regional windows and significantly improves the network’s ability to perceive regional-level features. By leveraging the local extraction capabilities of CNN in HMB, MS-Mamba can capture multi-scale representations. Moreover, to further enhance the capabilities in reconstructing details, a novel Adaptive Gradient Block (AGB) is proposed to explicitly guide the network in modeling detailed features by capturing various directional gradients. Concurrently, a Residual Fourier Block (RFB) is introduced to improve the network’s effectiveness in extracting fine textures in the frequency domain. Extensive experiments demonstrate that our MS-Mamba significantly surpasses existing state-of-the-art (SOTA) image restoration methods in four classic image restoration tasks with low computational complexity.

The contribution can be summarized as follows:

- We propose a novel multi-scale State-Space Model with UNet architecture, MS-Mamba, to effectively extract multi-scale features for high-quality image restoration.
- We propose a novel Hierarchical Mamba Block, which includes a global and regional State-Space Model (SSM) module to facilitate the capture of global and regional features through state-space functions. Furthermore, an Adaptive Gradient Block (AGB) and a Residual Fourier Block (RFB) are introduced to enhance the network’s detail extraction capabilities by capturing gradients in various directions and learning in the frequency domain.
- Extensive experiments on nine public benchmarks of four image restoration tasks demonstrate our proposed method outperforms existing state-of-the-art methods with low computational complexity.

Related Work

Image Restoration

Image restoration aims to remove undesired degradations (*e.g.* noise, blur, haze, rain *etc.*) in corrupted images. With the development of deep learning, lots of works (Fu et al. 2017; Ren et al. 2019; Yi et al. 2021; Zhang, Zhang, and Guo 2019; Peng et al. 2021, 2024; He et al. 2024) have been proposed and gained popularity over traditional methods (Li et al. 2016). In these methods, the encoder-decoder architecture is the most common framework since it can capture multi-scale features. Additionally, other techniques such as residual connections, various attention modules, and dilated convolutions (Li et al. 2018b; Peng et al. 2020; Shen et al. 2023; Wu et al. 2024; Xu et al. 2022) have been incorporated to extract richer and more important features and expand the receptive field of CNN. Despite their success, CNN-based restoration methods typically have difficulties in effectively modeling global dependencies, leading to performance bottlenecks and insufficient structural reconstruction capabilities. Therefore, transformer-based models have been proposed for image restoration. For instance, Wang et al. introduce a high-performing transformer-based network called Uformer (Wang et al. 2022) for image restoration. However, it incurs very high computational costs due to the quadratic computational complexity of the self-attention mechanism. To address this issue, window-based transformer networks have been proposed to reduce the computational burden. For example, Liang et al. propose a strong baseline model, SwinIR (Liang et al. 2021), for image restoration based on the Swin Transformer. Similarly, Zamir et al. design Restormer (Zamir et al. 2022), which calculates self-attention alongside the channel dimension. However, these methods cannot completely solve the high computational complexity of the attention mechanism. In this paper, we solve the quadratic complexity problem of the self-attention mechanism through State Space Models.

State Space Models

State Space Models (SSMs), originating from classical control theory, have been introduced to the Natural Language Processing (NLP) and CV (Computer Vision) field as a competitive backbone since SSMs learn global information at a low cost, i.e., with linear complexity. For example, as a landmark work, Mamba (Gu and Dao 2023) used a data-dependent SSM with a selection mechanism to learn global information, which outperforms traditional Transformer-based methods in NLP. With the success of SSMs in NLP tasks, SSMs have also been applied to computer vision tasks (Zhang et al. 2024; Liang et al. 2024; Guo et al. 2024; Zheng and Wu 2024; Zou et al. 2024). In image restoration, Guo et al. adopted SSMs to replace the Transformer in SwinIR and proposed MambaIR (Guo et al. 2024) for image restoration. However, MambaIR only computes SSMs at a single scale, which makes it difficult to effectively capture multi-scale features. Therefore, in this paper, we propose a Hierarchical Mamba Block, which can use the window and global SSM block to perceive regional-level features and global contextual information.

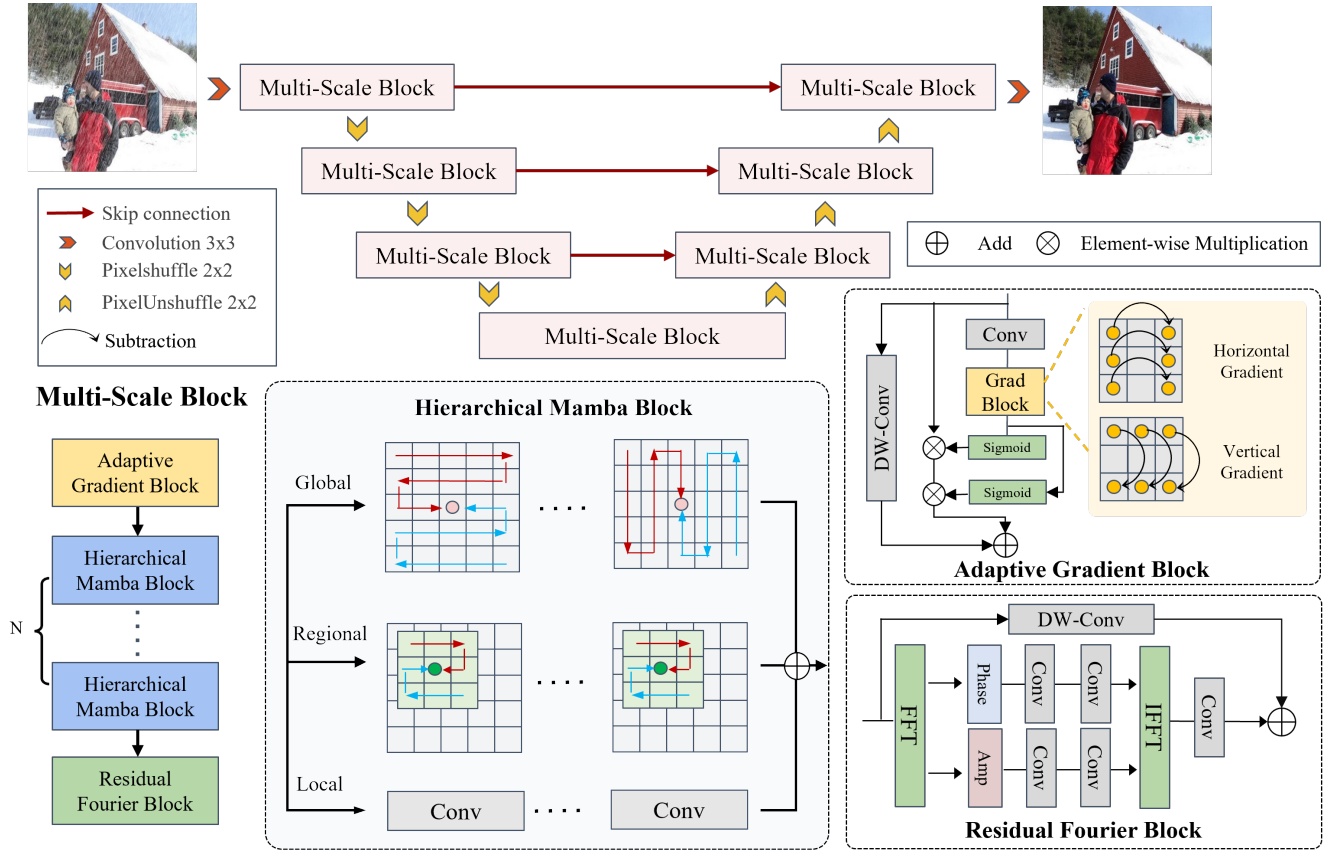


Figure 2: Architecture of our proposed MS-Mamba, which adopts a multi-scale UNet architecture and comprises of the novel Hierarchical Mamba Block, Adaptive Gradient Block, and Residual Fourier Block.

Method

In this section, we present the overall network pipeline of our proposed MS-Mamba, which leverages multi-scale representation learning to handle degradations at various scales in real-world scenarios for restoring image details and contrast. As shown in Fig. 2, our proposed MS-Mamba employs a multi-scale UNet architecture, which is composed of several fundamental modules dubbed Multi-Scale Blocks. Each Multi-Scale Block primarily contains three key and novel components: the Hierarchical Mamba Block, the Adaptive Gradient Block, and the Residual Fourier Block. These components are proposed to improve the representation capacity of multi-scale details by extracting multi-scale representations and fine-grained gradient information and learning from the frequency domain. Specifically, given input I , we first use a 3×3 convolution to extract shallow features F_s , which are then processed by the Multi-Scale Blocks. Finally, a 3×3 convolution maps the output features of the multi-scale U-Net to the restored high-quality image B . Next, we will detail the proposed Multi-Scale Block.

State Space Models

We commence with an exploration of the foundational principles underlying State Space Models (SSM). SSM is con-

ventionally conceptualized as linear time-invariant systems, mapping inputs $x(t) \in \mathbb{R}$ to outputs $y(t) \in \mathbb{R}$ via a latent state $h(t) \in \mathbb{R}^N$, where N denotes the dimensionality of the state space. Formally, such systems are characterized by linear ordinary differential equations, as specified in follows:

$$\begin{aligned} h'(t) &= Ah(t) + Bx(t) \\ y(t) &= Ch(t) + Dx(t), \end{aligned} \quad (1)$$

where the parameters include $A \in \mathbb{C}^{N \times N}$, $B, C \in \mathbb{C}^N$, and a skip connection $D \in \mathbb{C}^1$. Their discrete analogs, exemplified by models like Mamba (Gu and Dao 2023), utilize the zero-order hold (ZOH) method for discretization. This technique enhances the models' capacity to dynamically scan and adjust to input data through a selective scanning mechanism, which is especially advantageous for complex tasks such as image restoration. As a result, MambaIR is proposed. However, it only computes SSMs at a single scale, which limits its ability to capture multi-scale features. Therefore, we propose a Hierarchical Mamba Block to utilize the window and global SSM modules to perceive regional-level features and global contextual information.

Hierarchical Mamba Block

In real-world scenarios, degradations frequently exhibit multi-scale characteristics, requiring effective multi-scale

Methods	Rain200L		Rain200H		DID-Data		DDN-Data		SPA-Data		Average	
	PSNR \uparrow	SSIM \uparrow	PSNR \uparrow	SSIM \uparrow	PSNR \uparrow	SSIM \uparrow	PSNR \uparrow	SSIM \uparrow	PSNR \uparrow	SSIM \uparrow	PSNR \uparrow	SSIM \uparrow
DDN	34.68	0.9671	26.05	0.8056	30.97	0.9116	30.00	0.9041	36.16	0.9457	31.57	0.9068
RESCAN	36.09	0.9697	26.75	0.8353	33.38	0.9417	31.94	0.9345	38.11	0.9707	33.25	0.9304
PReNet	37.80	0.9814	29.04	0.8991	33.17	0.9481	32.60	0.9459	40.16	0.9816	34.55	0.9512
MSPFN	38.58	0.9827	29.36	0.9034	33.72	0.9550	32.99	0.9333	43.43	0.9843	35.62	0.9517
RCDNet	39.17	0.9885	30.24	0.9048	34.08	0.9532	33.04	0.9472	43.36	0.9831	35.98	0.9554
MPRNet	39.47	0.9825	30.67	0.9110	33.99	0.9590	33.10	0.9347	43.64	0.9844	36.17	0.9543
SwinIR	40.61	0.9871	31.76	0.9151	34.07	0.9313	33.16	0.9312	44.97	0.9890	36.91	0.9507
DualGCN	40.73	0.9886	31.15	0.9125	34.37	0.9620	33.01	0.9489	44.18	0.9902	36.69	0.9604
SPDNet	40.50	0.9875	31.28	0.9207	34.57	0.9560	33.15	0.9457	43.20	0.9871	36.54	0.9594
Uformer	40.20	0.9860	30.80	0.9105	35.02	0.9621	33.95	0.9545	46.13	0.9913	37.22	0.9609
Restormer	40.99	0.9890	32.00	0.9329	35.29	0.9641	34.20	0.9571	47.98	0.9921	38.09	0.9670
IDT	40.74	0.9884	32.10	<u>0.9344</u>	34.89	0.9623	33.84	0.9549	47.35	<u>0.9930</u>	37.78	0.9666
DLINet	40.91	0.9886	31.47	0.9231	-	-	33.61	0.9514	44.94	0.9885	37.73	0.9629
DRSformer	<u>41.23</u>	0.9894	32.17	0.9326	<u>35.35</u>	<u>0.9646</u>	<u>34.35</u>	<u>0.9588</u>	<u>48.54</u>	0.9924	<u>38.33</u>	<u>0.9676</u>
MambaIR	41.13	<u>0.9895</u>	<u>32.18</u>	0.9295	35.05	0.9612	34.00	0.9554	46.03	0.9902	37.68	0.9652
Ours	41.88	0.9904	32.24	0.9365	35.48	0.9656	34.45	0.9601	49.06	0.9934	38.62	0.9692

Table 1: Quantitative PSNR \uparrow and SSIM \uparrow comparisons with existing state-of-the-art image deraining methods. The **bold** and the underline represent the best and the second-best performance, respectively.

information representation for image restoration. To achieve this, we propose a novel Hierarchical Mamba Block (HMB), which integrates both State Space Models (SSM) and CNN to efficiently capture global, regional, and local representations. While transformer is a common choice for global representation, their computational demands are substantial. Therefore, we employ the Visual State Space (VSS) block (Liu et al. 2024), an efficient global SSM that uses a 2D scanning method to model spatial relationships in both horizontal and vertical directions for global sequence modeling.

While the global SSM provides long-range modeling capabilities, it is prone to catastrophic forgetting, leading to insufficient representation of regional and local areas, which are crucial for effective image restoration. To overcome this limitation, we propose a novel regional Window SSM Module, specifically designed to capture regional-scale representations. Specifically, we first partition the image into multiple distinct local windows. For the features within each local window, we perform a linear projection of the sequence and construct sequences in both forward and backward directions to enhance the receptive field. Finally, we compute the output using the SSM.

Despite the aforementioned two SSM modules offer robust global and regional representation modeling capabilities, local representation is essential for perceiving fine-grained degradations. However, directly reducing the window size in the Window SSM Module significantly increases the number of windows, leading to substantial computational complexity. To address this, we employ Convolutional Neural Networks (CNN), a classical approach for extracting local representations, which facilitates the network’s ability to learn fine-grained features in local regions. For a given input feature F_{in} , the computation process of the HMB can be succinctly represented as:

$$F_{out} = GSSM((F_{in}) + RSSM((F_{in}) + \text{Conv}(F_{in})), \quad (2)$$

where $GSSM$ and $RSSM$ denote the global and regional SSM module, respectively. A comprehensive discussion on the global and regional SSM modules is provided in the

Appendix A.1. While the proposed HMB is adept at managing multi-scale features, it lacks the crucial detail modeling capability for image restoration. Therefore, we introduce the Adaptive Gradient Block (AGB) and the Residual Fourier Block (RFB). The AGB is designed to capture gradient details in various directions, whereas the RFB operates in the frequency domain to improve the modeling capacity of multi-scale details.

Adaptive Gradient Block

To improve the network’s ability to extract fine textures, we propose a novel Adaptive Gradient Block (AGB) to capture gradients in various directions, as shown in Fig. 2. Specifically, a gradient block is introduced in AGB to extract features in both horizontal and vertical directions, as illustrated by the following equations:

$$\begin{aligned} F_x &= F_{in}(x+1, y) - F_{in}(x-1, y), \\ F_y &= F_{in}(x, y+1) - F_{in}(x, y-1), \\ \nabla F &= (F_x, F_y), \\ G &= \|\nabla F\|_2, \end{aligned} \quad (3)$$

where F_{in} denotes the input feature, and G represents the gradient map of F_{in} . The variables x and y refer to the coordinate indices. Then, leveraging the gradient information from different directions, the AGB generates channel and spatial detail attention maps through the sigmoid activation function to provide the network with the ability to perceive spatial details and detail-related channels, thereby improving the network’s overall detail reconstruction capability for degraded images. The above process can be represented as:

$$\begin{aligned} F_{in} &= \text{ReLU}(\text{Conv}(G)), \\ \mathbf{A}_c &= f_{ca}(F_{in}) \in \mathbb{R}^{C \times 1 \times 1}, \\ \mathbf{A}_s &= f_{sa}(F_{in}) \in \mathbb{R}^{1 \times H \times W}, \\ \hat{F} &= \mathbf{A}_s(\mathbf{A}_c(I)) + \text{DW-Conv}(I), \end{aligned} \quad (4)$$

where \mathbf{A}_c , \mathbf{A}_s are the channel and spatial attention maps, respectively. DW-Conv denotes the depth-wise convolution.

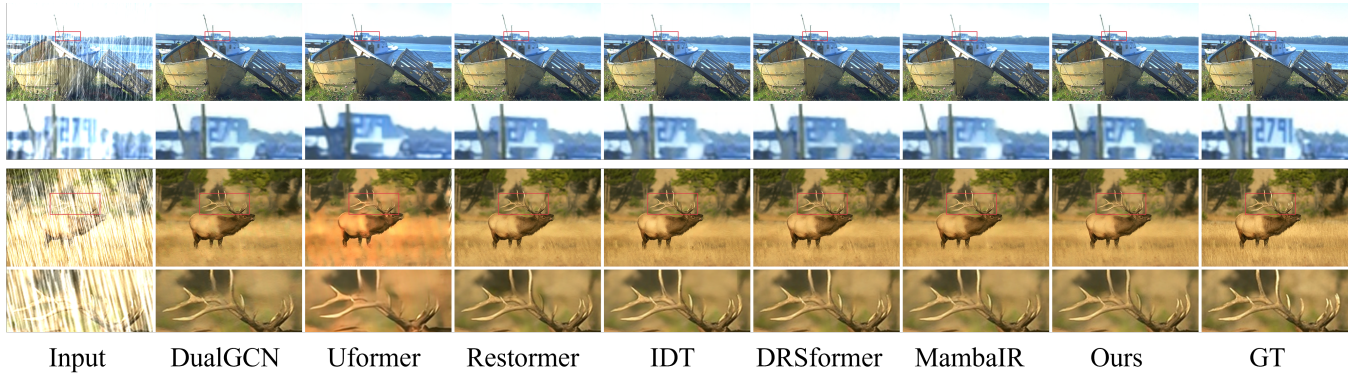


Figure 3: Visual comparison on the synthetic rainy images from the Rain200H (Yang et al. 2017) dataset. Zooming in the figures offers a better view. Our proposed method effectively removes rain streaks and delivers the most visually pleasing results.

Methods	DeHamer	PMNet	MAXIM	Restormer	DehazeFormer-L	MDFEN	MITNet	FocalNet	UMamba	Ours
PSNR \uparrow	36.63	38.41	38.11	38.88	40.05	37.14	40.23	<u>40.82</u>	40.17	41.55
SSIM \uparrow	0.988	0.990	0.991	0.991	0.996	0.989	0.992	0.996	<u>0.996</u>	0.996

Table 2: Quantitative comparisons with state-of-the-art dehaze methods on the benchmark SOTS-Indoor (Li et al. 2018a).

Residual Fourier Block

Recognizing that the spatial domain predominantly resides in low-frequency information, rendering high-frequency details challenging for network capture, we propose a novel Residual Fourier Block (RFB) to enhance fine texture extraction in the frequency domain, as shown in the bottom right corner of Fig. 2. Specifically, the RFB transforms the input feature into the Fourier domain, yielding separate amplitude and phase components. Recognizing the distinct contributions of the amplitude and phase components in degradation, they are processed separately in RFB. Two sequential 1×1 convolutional layers, followed by the ReLU activation function, are used for the processing. After that, the processed amplitude and phase components are transformed back into the spatial domain, which is then followed by a 3×3 convolutional layer. Additionally, a residual depth-wise convolution consolidates frequency information, aiding in the preservation of high-frequency details crucial for image clarity often diminished during restoration.

Loss Function

Following previous works (Zamir et al. 2022; Chen et al. 2023), we utilize the common L1 loss \mathcal{L}_1 for training. Furthermore, to enhance the network’s ability to capture details, we also employ the edge loss \mathcal{L}_{edge} and the frequency loss \mathcal{L}_{fft} . The total loss is presented as follows:

$$\mathcal{L}_{total} = \lambda_1 \mathcal{L}_1(\mathcal{B}, \mathcal{B}_{gt}) + \lambda_2 \mathcal{L}_{edge}(\mathcal{B}, \mathcal{B}_{gt}) + \lambda_3 \mathcal{L}_{fft}(\mathcal{B}, \mathcal{B}_{gt}), \quad (5)$$

where \mathcal{B} and \mathcal{B}_{gt} denote the predicted output and the corresponding ground truth, respectively. The parameters λ_1 , λ_2 , and λ_3 are balancing factors. In our experiments, we set λ_1 , λ_2 , and λ_3 to 1, 0.1, and 0.05, respectively.

Method	LOL-v2-real		LOL-v2-syn	
	PSNR \uparrow	SSIM \uparrow	PSNR \uparrow	SSIM \uparrow
RetinexNet	15.47	0.567	17.13	0.798
KinD	14.74	0.641	13.29	0.578
RUAS	18.37	0.723	16.55	0.652
Uformer	18.82	0.771	19.66	0.871
Sparse	20.06	0.816	22.05	0.905
Restormer	19.94	0.827	21.41	0.830
MIRNet	20.02	0.820	21.94	0.876
SNR-Net	21.48	<u>0.849</u>	24.14	0.928
Retinexformer	22.80	0.840	<u>25.67</u>	0.930
FreqMamba	-	-	24.46	0.936
LYT-Net	<u>22.93</u>	0.840	23.33	0.905
Ours	26.69	0.896	26.62	0.947

Table 3: Comparisons of low-light image enhancement methods on the LOL-v2 (Yang et al. 2021b) benchmarks.

Experiments

Experimental Settings

Datasets. To comprehensively verify the superiority of our method in image restoration, we conduct comparison experiments on nine public benchmarks across four classic image restoration tasks. For Image Deraining, following (Chen et al. 2023), we evaluate on five public benchmarks: Rain200L/H, DID-Data, DDN-Data, and SPA-Data, where SPA-Data is a real-world dataset. For Image Dehazing, following (Song et al. 2023), we evaluate on the public benchmark SOTS-indoor. For Low-light Image Enhancement, we evaluate on the public LOL-v2-real and LOL-v2-syn benchmarks, following (Cai et al. 2023). For Image Denoising, following (Guo et al. 2024), we evaluate on the public real-world SIDD benchmark. More details on the training and

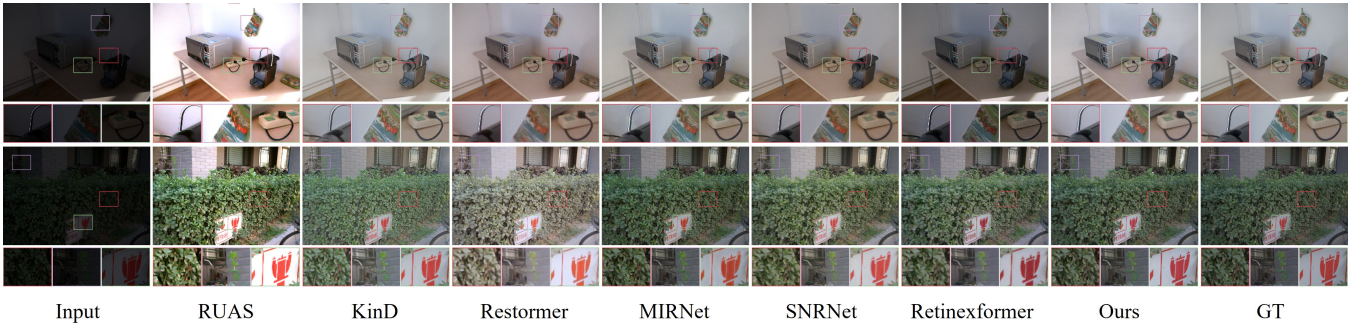


Figure 4: Visual comparison on the real low-light images from the LOLv2 (Yang et al. 2021b) dataset. Zooming in the figures offers a better view. Our proposed method delivers the most visually pleasing results.

Methods	CycleISP	MIRNet	DeamNet	MPRNet	DAGL	Uformer	VDIR	DRANet	MambaIR	Ours
PSNR \uparrow	39.52	39.72	39.47	39.71	39.77	39.77	39.26	39.50	<u>39.89</u>	39.92
SSIM \uparrow	0.957	0.959	0.957	0.958	0.959	0.959	0.955	0.957	<u>0.960</u>	0.960

Table 4: Quantitative comparisons of different denoising models on the SIDD (Abdelhamed, Lin, and Brown 2018) benchmark.

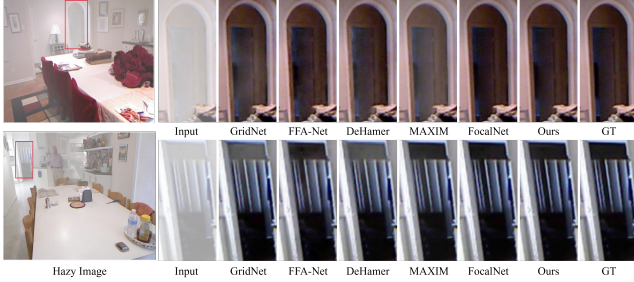


Figure 5: Image dehazing visual comparison on the SOTS-indoor (Li et al. 2018a) datasets. Best viewed on screen.

test sets are presented in the **Appendix A.3**.

Evaluation Metrics. We use PSNR and SSIM to evaluate the performance. Specifically, we follow (Zamir et al. 2022) to evaluate on the Y channel for image deraining and denoising. For image dehazing and low-light enhancement, we evaluate on the RGB channel, following (Cui et al. 2023) and (Cai et al. 2023), respectively. Note that higher values of PSNR and SSIM indicate better restoration quality.

Implementation Details. Our model employs a 4-level encoder-decoder U-Net architecture, with the number of blocks in each stage set to [2, 2, 2, 2] and the number of feature channels C set to 48. The window size for the regional SSM Module is configured as [16, 16, 8, 8]. Network parameters are optimized using the AdamW optimizer, starting with an initial learning rate of 3×10^{-4} for the first 92K iterations, followed by a reduction to 1×10^{-6} over the subsequent 208,000 iterations, employing a cosine annealing strategy. Additionally, random flips and rotations are applied for data augmentation. Experiments are conducted using the PyTorch framework on four NVIDIA GeForce RTX 3090 GPUs. More details are available in the **Appendix A.2**.

Comparisons with State-of-the-art Methods. *Image Deraining:* we compare our method against fifteen state-of-the-art methods, including: DDN, RESCAN, PReNet, MSPFN, RCDNet, MPRNet, SwinIR, DualGCN, SPDNet, Uformer, Restormer, IDT, DLINet, DRSformer and MambaIR. *Image Dehazing:* we conduct comparisons with nine state-of-the-art methods, including: DeHamer, PM-Net, MAXIM, Restormer, DehazeFormer, MDFEN, MIT-Net, FocalNet and UMamba. *Low-light Enhancement:* we evaluate our approach against eleven state-of-the-art methods, including: Uformer, RetinexNet, Sparse, RUAS, KinD, Restormer, MIRNet, SNRNet, Retinexformer, FreqMamba and LYTNet. *Image Denoising:* we evaluate our approach against nine state-of-the-art methods, including: CycleISP, MIRNet, DeamNet, MPRNet, DAGL, Uformer, VDIR, DRANet and MambaIR.

Quantitative and Qualitative Results

To validate the effectiveness of our proposed method, we conduct experiments on four restoration tasks across a total of nine public benchmarks, as shown in Tables 1, 2, 3, 4. *Image Deraining:* Our method achieves the best performance on all five benchmarks for image deraining. For example, on Rain200L, our method surpasses the existing state-of-the-art (SOTA) method DRSformer by 0.65 dB in PSNR. For the real-world dataset SPA-Data, our MS-Mamba outperforms existing methods by 0.52 dB. *Image Dehazing:* Our method also achieves the best performance on the SOTS-Indoor benchmarks for image dehazing. For example, MS-Mamba demonstrates a 1.38 dB improvement over the SSM-based method Umamba. *Low-light Image Enhancement:* As indicated in Table 3, our model consistently achieves the best performance across all variants of the LOLv2 dataset. For instance, MS-Mamba achieves a 2.16 dB gain over the SSM-based method FreqMamba on the LOL-v2-syn benchmark. *Image Denoising:* Similarly, our method achieves the

Methods	DeHamer	Uformer	Restormer	MIRNet	IDT	DehazeFormer-L	DRSformer	UMamba	MambaIR	Ours
Params(M) ↓	132.450	50.880	26.127	31.760	16.420	25.452	33.660	19.250	31.506	19.640
FLOPs(G) ↓	48.926	86.891	154.882	785.000	73.474	279.624	242.989	173.550	161.902	117.524

Table 5: Comparisons of model complexity against state-of-the-art methods. The input size is 256×256 pixels.

Global	Regional	Local	PSNR ↑	SSIM ↑
✓			40.85	0.9844
	✓		41.09	0.9888
		✓	36.76	0.9757
✓	✓		41.75	0.9901
✓		✓	41.41	0.9898
	✓	✓	41.55	0.9900
✓	✓	✓	41.88	0.9904

Table 6: Ablation study for Hierarchical Mamba Block.

best performance on the real-world SIDD benchmark for image denoising. Additionally, to demonstrate the visual superiority of the proposed method, we present some visual comparisons on the Rain200H deraining dataset in Fig. 3, the SOTS-indoor dehazing dataset in Fig. 5, and the low-light enhancement LOLv2 dataset in Fig. 4. These results demonstrate the superiority and generality of the proposed method across various image restoration tasks. More visualization comparisons are presented in the **Appendix A.5**.

Comparison of model complexity

In practical deployment, model complexity is of paramount importance. Therefore, we conduct a comparative analysis of our method against existing state-of-the-art approaches in terms of model parameters and floating point operations (FLOPs), as presented in Table. 5. The results indicate that, compared to all existing methods, our model exhibits fewer parameters and lower FLOPs while achieving superior performance. For example, compared to the SSM-based method MambaIR, our model reduces the number of parameters by 11.866 M and has fewer FLOPs. Moreover, our FLOPs are reduced by 56.026 G compared to Umamba. This highlights the efficiency and practicality of our proposed method for real-world applications.

Ablation Study

To validate the effectiveness of our proposed Hierarchical Mamba Block, we conduct ablation experiments on the Rain200L dataset. Specifically, we remove each branch of the block and consider combinations of any two branches, subsequently evaluating their performance. The results are presented in Table 6. It can be observed that each scale is crucial for the HMB. For instance, when using only the global and regional scales, the PSNR drops by 1.03 dB and 0.79 dB, respectively; when using only the local scale, the PSNR decreases significantly by 5.12 dB. Moreover, when any two of the three scales are present, the performance also declines. These experimental results demonstrate the importance of multi-scale information in the proposed HMB. Additional ablation studies, including various AGB variants,

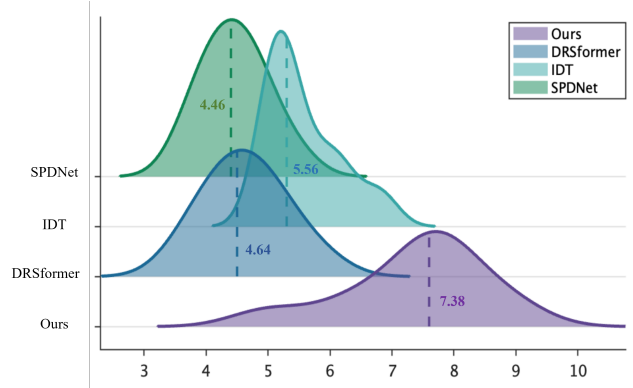


Figure 6: Results of the user study on the Real127 Dataset.

the effectiveness of RFB, and the loss function configurations, are detailed in **Appendix A.4**.

User Study

To validate the superiority of our method on real-world scenes, a user study is conducted. Specifically, we randomly select 10 rainy images from the Real127 dataset (Zhang and Patel 2018). Ten participants rate each image from 0 (not removed at all) to 10 (very clean). The aggregated results, as shown in Fig. 6, indicate that existing methods struggle with adaptive rain removal, resulting in lower user satisfaction. In contrast, our method effectively eliminates degradations, achieving the highest average score of 7.38, and demonstrating superior generalization in real-world scenarios.

Conclusion

In this paper, we propose MS-Mamba, an efficient multi-scale SSM with U-Net architecture designed to effectively capture multi-scale features for high-quality image restoration. MS-Mamba effectively captures global contextual information through the proposed global SSM module, enhances regional feature perception capacity via the proposed regional SSM module, and extracts local features using CNN. Additionally, an Adaptive Gradient Block (AGB) and a Residual Fourier Block (RFB) are introduced to enhance the network’s detail extraction capabilities by capturing gradients from various directions and learning in the frequency domain. Extensive experiments demonstrate that MS-Mamba significantly outperforms existing SOTA methods on nine public benchmarks and real scenarios across four classic image restoration tasks while maintaining low computational complexity.

References

- Abdelhamed, A.; Lin, S.; and Brown, M. S. 2018. A high-quality denoising dataset for smartphone cameras. In *Proceedings of the IEEE conference on computer vision and pattern recognition*, 1692–1700.
- Brateanu, A.; Balmez, R.; Avram, A.; and Orhei, C. 2024. LYT-Net: Lightweight YUV Transformer-based Network for Low-Light Image Enhancement. *arXiv preprint arXiv:2401.15204*.
- Cai, Y.; Bian, H.; Lin, J.; Wang, H.; Timofte, R.; and Zhang, Y. 2023. Retinexformer: One-stage retinex-based transformer for low-light image enhancement. In *Proceedings of the IEEE/CVF International Conference on Computer Vision*, 12504–12513.
- Chen, W.; Wenjing, W.; Wenhao, Y.; and Jiaying, L. 2018. Deep Retinex Decomposition for Low-Light Enhancement. In *British Machine Vision Conference*.
- Chen, X.; Li, H.; Li, M.; and Pan, J. 2023. Learning a Sparse Transformer Network for Effective Image Deraining. In *Proceedings of the IEEE/CVF Conference on Computer Vision and Pattern Recognition (CVPR)*, 5896–5905.
- Cui, Y.; Ren, W.; Cao, X.; and Knoll, A. 2023. Focal network for image restoration. In *Proceedings of the IEEE/CVF international conference on computer vision*, 13001–13011.
- Fu, X.; Huang, J.; Zeng, D.; Huang, Y.; Ding, X.; and Paisley, J. 2017. Removing rain from single images via a deep detail network. In *Proceedings of the IEEE conference on computer vision and pattern recognition*, 3855–3863.
- Fu, X.; Qi, Q.; Zha, Z.-J.; Zhu, Y.; and Ding, X. 2021. Rain streak removal via dual graph convolutional network. In *Proceedings of the AAAI Conference on Artificial Intelligence*, volume 35, 1352–1360.
- Gu, A.; and Dao, T. 2023. Mamba: Linear-time sequence modeling with selective state spaces. *arXiv preprint arXiv:2312.00752*.
- Guo, C.-L.; Yan, Q.; Anwar, S.; Cong, R.; Ren, W.; and Li, C. 2022. Image dehazing transformer with transmission-aware 3d position embedding. In *Proceedings of the IEEE/CVF conference on computer vision and pattern recognition*, 5812–5820.
- Guo, H.; Li, J.; Dai, T.; Ouyang, Z.; Ren, X.; and Xia, S.-T. 2024. MambaIR: A Simple Baseline for Image Restoration with State-Space Model. *arXiv preprint arXiv:2402.15648*.
- He, Y.; Peng, L.; Wang, L.; and Cheng, J. 2024. Latent Degradation Representation Constraint for Single Image Deraining. In *ICASSP 2024-2024 IEEE International Conference on Acoustics, Speech and Signal Processing (ICASSP)*, 3155–3159. IEEE.
- Jiang, K.; Wang, Z.; Yi, P.; Chen, C.; Huang, B.; Luo, Y.; Ma, J.; and Jiang, J. 2020. Multi-scale progressive fusion network for single image deraining. In *Proceedings of the IEEE/CVF conference on computer vision and pattern recognition*, 8346–8355.
- Khudjaev, N.; Tsoy, R.; A Sharif, S.; Myrzabekov, A.; Kim, S.; and Lee, J. 2024. Dformer: Learning Efficient Image Restoration with Perceptual Guidance. In *Proceedings of the IEEE/CVF Conference on Computer Vision and Pattern Recognition*, 6363–6372.
- Li, B.; Ren, W.; Fu, D.; Tao, D.; Feng, D.; Zeng, W.; and Wang, Z. 2018a. Benchmarking single-image dehazing and beyond. *IEEE Transactions on Image Processing*, 28(1): 492–505.
- Li, W.; Chen, G.; and Chang, Y. 2023. An Efficient Single Image De-Raining Model With Decoupled Deep Networks. *IEEE Transactions on Image Processing*, 33: 69–81.
- Li, X.; Wu, J.; Lin, Z.; Liu, H.; and Zha, H. 2018b. Recurrent squeeze-and-excitation context aggregation net for single image deraining. In *Proceedings of the European conference on computer vision (ECCV)*, 254–269.
- Li, Y.; Tan, R. T.; Guo, X.; Lu, J.; and Brown, M. S. 2016. Rain streak removal using layer priors. In *Proceedings of the IEEE conference on computer vision and pattern recognition*, 2736–2744.
- Liang, D.; Zhou, X.; Wang, X.; Zhu, X.; Xu, W.; Zou, Z.; Ye, X.; and Bai, X. 2024. PointMamba: A Simple State Space Model for Point Cloud Analysis. *arXiv preprint arXiv:2402.10739*.
- Liang, J.; Cao, J.; Sun, G.; Zhang, K.; Van Gool, L.; and Timofte, R. 2021. Swinir: Image restoration using swin transformer. In *Proceedings of the IEEE/CVF international conference on computer vision*, 1833–1844.
- Liu, R.; Ma, L.; Zhang, J.; Fan, X.; and Luo, Z. 2021. Retinex-inspired unrolling with cooperative prior architecture search for low-light image enhancement. In *Proceedings of the IEEE/CVF conference on computer vision and pattern recognition*, 10561–10570.
- Liu, Y.; Tian, Y.; Zhao, Y.; Yu, H.; Xie, L.; Wang, Y.; Ye, Q.; and Liu, Y. 2024. Vmamba: Visual state space model. *arXiv preprint arXiv:2401.10166*.
- Mao, X.; Liu, Y.; Shen, W.; Li, Q.; and Wang, Y. 2021. Deep residual fourier transformation for single image deblurring. *arXiv preprint arXiv:2111.11745*, 2(3): 5.
- Mehri, A.; Ardakani, P. B.; and Sappa, A. D. 2021. MPRNet: Multi-path residual network for lightweight image super resolution. In *Proceedings of the IEEE/CVF Winter Conference on Applications of Computer Vision*, 2704–2713.
- Mou, C.; Zhang, J.; and Wu, Z. 2021. Dynamic attentive graph learning for image restoration. In *Proceedings of the IEEE/CVF international conference on computer vision*, 4328–4337.
- Peng, L.; Cao, Y.; Sun, Y.; and Wang, Y. 2024. Lightweight Adaptive Feature De-drifting for Compressed Image Classification. *IEEE Transactions on Multimedia*.
- Peng, L.; Jiang, A.; Wei, H.; Liu, B.; and Wang, M. 2021. Ensemble single image deraining network via progressive structural boosting constraints. *Signal Processing: Image Communication*, 99: 116460.
- Peng, L.; Jiang, A.; Yi, Q.; and Wang, M. 2020. Cumulative rain density sensing network for single image derain. *IEEE Signal Processing Letters*, 27: 406–410.
- Qu, J.; Liu, R. W.; Gao, Y.; Guo, Y.; Zhu, F.; and Wang, F.-Y. 2024. Double domain guided real-time low-light image

- enhancement for ultra-high-definition transportation surveillance. *IEEE Transactions on Intelligent Transportation Systems*.
- Ren, C.; He, X.; Wang, C.; and Zhao, Z. 2021. Adaptive consistency prior based deep network for image denoising. In *Proceedings of the IEEE/CVF conference on computer vision and pattern recognition*, 8596–8606.
- Ren, D.; Zuo, W.; Hu, Q.; Zhu, P.; and Meng, D. 2019. Progressive image deraining networks: A better and simpler baseline. In *Proceedings of the IEEE/CVF conference on computer vision and pattern recognition*, 3937–3946.
- Shen, H.; Zhao, Z.-Q.; Zhang, Y.; and Zhang, Z. 2023. Mutual information-driven triple interaction network for efficient image dehazing. In *Proceedings of the 31st ACM International Conference on Multimedia*, 7–16.
- Soh, J. W.; and Cho, N. I. 2022. Variational Deep Image Restoration. *IEEE Transactions on Image Processing*, 31: 4363–4376.
- Song, Y.; He, Z.; Qian, H.; and Du, X. 2023. Vision transformers for single image dehazing. *IEEE Transactions on Image Processing*, 32: 1927–1941.
- Tu, Z.; Talebi, H.; Zhang, H.; Yang, F.; Milanfar, P.; Bovik, A.; and Li, Y. 2022. Maxim: Multi-axis mlp for image processing. In *Proceedings of the IEEE/CVF conference on computer vision and pattern recognition*, 5769–5780.
- Wang, H.; Xie, Q.; Zhao, Q.; and Meng, D. 2020. A model-driven deep neural network for single image rain removal. In *Proceedings of the IEEE/CVF conference on computer vision and pattern recognition*, 3103–3112.
- Wang, Z.; Cun, X.; Bao, J.; Zhou, W.; Liu, J.; and Li, H. 2022. Uformer: A general u-shaped transformer for image restoration. In *Proceedings of the IEEE/CVF conference on computer vision and pattern recognition*, 17683–17693.
- Wu, W.; Liu, S.; Xia, Y.; and Zhang, Y. 2024. Dual residual attention network for image denoising. *Pattern Recognition*, 149: 110291.
- Xiao, J.; Fu, X.; Liu, A.; Wu, F.; and Zha, Z.-J. 2022. Image de-raining transformer. *IEEE Transactions on Pattern Analysis and Machine Intelligence*.
- Xu, X.; Wang, R.; Fu, C.-W.; and Jia, J. 2022. SNR-aware low-light image enhancement. In *Proceedings of the IEEE/CVF conference on computer vision and pattern recognition*, 17714–17724.
- Yang, W.; Tan, R. T.; Feng, J.; Liu, J.; Guo, Z.; and Yan, S. 2017. Deep joint rain detection and removal from a single image. In *Proceedings of the IEEE conference on computer vision and pattern recognition*, 1357–1366.
- Yang, W.; Wang, W.; Huang, H.; Wang, S.; and Liu, J. 2021a. Sparse gradient regularized deep retinex network for robust low-light image enhancement. *IEEE Transactions on Image Processing*, 30: 2072–2086.
- Yang, W.; Wang, W.; Huang, H.; Wang, S.; and Liu, J. 2021b. Sparse gradient regularized deep retinex network for robust low-light image enhancement. *IEEE Transactions on Image Processing*, 30: 2072–2086.
- Ye, T.; Zhang, Y.; Jiang, M.; Chen, L.; Liu, Y.; Chen, S.; and Chen, E. 2022. Perceiving and modeling density for image dehazing. In *European conference on computer vision*, 130–145. Springer.
- Yi, Q.; Li, J.; Dai, Q.; Fang, F.; Zhang, G.; and Zeng, T. 2021. Structure-preserving deraining with residue channel prior guidance. In *Proceedings of the IEEE/CVF international conference on computer vision*, 4238–4247.
- Yin, X.; Tu, G.; and Chen, Q. 2023. Multiscale depth fusion with contextual hybrid enhancement network for image dehazing. *IEEE Transactions on Instrumentation and Measurement*.
- Yu, H.; Zheng, N.; Zhou, M.; Huang, J.; Xiao, Z.; and Zhao, F. 2022. Frequency and spatial dual guidance for image dehazing. In *European Conference on Computer Vision*, 181–198. Springer.
- Zamir, S. W.; Arora, A.; Khan, S.; Hayat, M.; Khan, F. S.; and Yang, M.-H. 2022. Restormer: Efficient transformer for high-resolution image restoration. In *Proceedings of the IEEE/CVF conference on computer vision and pattern recognition*, 5728–5739.
- Zamir, S. W.; Arora, A.; Khan, S.; Hayat, M.; Khan, F. S.; Yang, M.-H.; and Shao, L. 2020a. CycleISP: Real Image Restoration via Improved Data Synthesis. In *Proceedings of the IEEE/CVF Conference on Computer Vision and Pattern Recognition (CVPR)*.
- Zamir, S. W.; Arora, A.; Khan, S.; Hayat, M.; Khan, F. S.; Yang, M.-H.; and Shao, L. 2020b. Learning enriched features for real image restoration and enhancement. In *Computer Vision—ECCV 2020: 16th European Conference, Glasgow, UK, August 23–28, 2020, Proceedings, Part XXV 16*, 492–511. Springer.
- Zhang, C.; Huang, Z.; Tung, B. X. L.; Ang, M. H.; and Rus, D. 2023. SmartRainNet: Uncertainty Estimation For Laser Measurement in Rain. In *2023 IEEE International Conference on Robotics and Automation (ICRA)*, 10567–10573. IEEE.
- Zhang, H.; and Patel, V. M. 2018. Density-aware single image de-raining using a multi-stream dense network. In *Proceedings of the IEEE conference on computer vision and pattern recognition*, 695–704.
- Zhang, M.; Yu, Y.; Gu, L.; Lin, T.; and Tao, X. 2024. Vm-unet-v2 rethinking vision mamba unet for medical image segmentation. *arXiv preprint arXiv:2403.09157*.
- Zhang, Y.; Zhang, J.; and Guo, X. 2019. Kindling the Darkness: A Practical Low-light Image Enhancer. In *Proceedings of the 27th ACM International Conference on Multimedia*, 1632–1640.
- Zheng, Z.; and Wu, C. 2024. U-shaped Vision Mamba for Single Image Dehazing. *arXiv:2402.04139*.
- Zou, Z.; Yu, H.; Huang, J.; and Zhao, F. 2024. FreqMamba: Viewing Mamba from a Frequency Perspective for Image Deraining. In *ACM Multimedia 2024*.